

NJC

New Journal of Chemistry

Accepted Manuscript

A journal for new directions in chemistry

This article can be cited before page numbers have been issued, to do this please use: T. Geng, C. Zhang, C. Hu, M. Liu, Y. Fei and H. Xia, *New J. Chem.*, 2020, DOI: 10.1039/C9NJ05509F.



This is an Accepted Manuscript, which has been through the Royal Society of Chemistry peer review process and has been accepted for publication.

Accepted Manuscripts are published online shortly after acceptance, before technical editing, formatting and proof reading. Using this free service, authors can make their results available to the community, in citable form, before we publish the edited article. We will replace this Accepted Manuscript with the edited and formatted Advance Article as soon as it is available.

You can find more information about Accepted Manuscripts in the [Information for Authors](#).

Please note that technical editing may introduce minor changes to the text and/or graphics, which may alter content. The journal's standard [Terms & Conditions](#) and the [Ethical guidelines](#) still apply. In no event shall the Royal Society of Chemistry be held responsible for any errors or omissions in this Accepted Manuscript or any consequences arising from the use of any information it contains.

The synthesis of 1,6-disubstituted pyrene-based conjugated microporous polymers for reversible adsorbing and fluorescent sensing to iodine

Received 00th January 20xx,
 Accepted 00th January 20xx

DOI: 10.1039/x0xx00000x

www.rsc.org/

Tong-Mou Geng^{a*}, Can Zhang^a, Chen Hu^a, Min Liu^a, Ya-Ting Fei^a, and Hong-Yu Xia^a

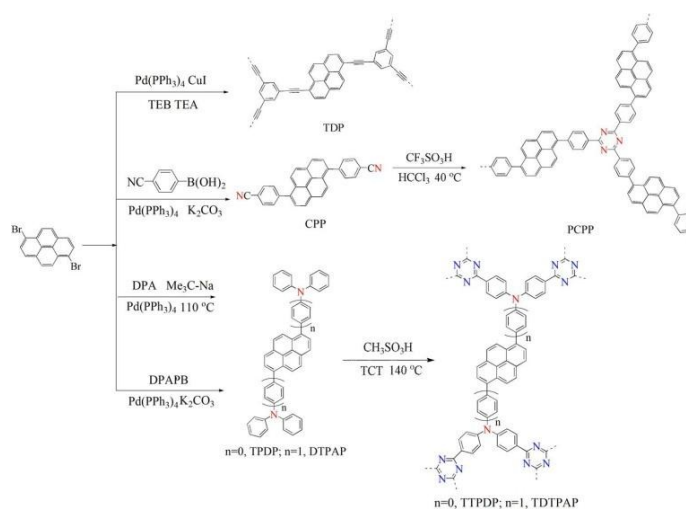
Abstract Here we present detailed evidence of highly efficient iodine capture and sensing in 1,6-disubstituted pyrene-based fluorescent conjugated microporous polymers, which were synthesized by a Sonogashira – Hagihara polycondensation reaction (TDP), trimerization reaction of bi-cyano compound (CPP) catalyzed using trifluoromethanesulfonic acid (PCPP), and Friedel-Crafts reaction catalyzed with $\text{CH}_3\text{SO}_3\text{H}$ (TTPDP and TDTPAP), respectively. TDP, PCPP, TTPDP, and TDTPAP have specific surface areas of 261.9, 43.0, 187.5, and 695.2 $\text{m}^2 \text{g}^{-1}$, and display reversible guest uptake of 0.61, 3.07, 3.49, 4.19 g g^{-1} in iodine vapor. The four CMPs exhibit high sensitivity and selectivity to iodine via fluorescence quenching. Furthermore, PCPP exhibited extremely high detection sensitivity to I_2 with K_{sv} of $1.40 \times 10^5 \text{ L mol}^{-1}$ and detection limit of $3.14 \times 10^{-13} \text{ mol L}^{-1}$. To the best of our knowledge, it displays the highest reported K_{sv} value and the lowest detection limit value to iodine to date.

Introduction

Porous organic polymers (POPs) have attracted considerable attention due to their many exciting potential applications.¹ Up to present, a variety of POPs have been developed, including polymers of intrinsic microporosity (PIMs),² porous aromatic frameworks (PAFs),³ hypercrosslinked polymers (HCPs),^{4,5} covalent triazine-based frameworks (CTFs),⁶ covalent organic frameworks (COFs),⁷ and conjugated microporous polymers (CMPs)⁸ and so on.

Pyrene is an efficient chromophore with excellent fluorescent quantum yield and efficient excimer emission that makes it useful as a fluorescence sensor. Many polymers based

on pyrene derivatives have been widely used as fluorescence sensors in many applications.⁹ The derivatives of pyrene were also used for building various CMPs used as gas adsorbents,¹⁰⁻¹² photocatalysts, fluorescence materials,^{13,14} and fluorescence sensors.¹⁵⁻¹⁷ Nevertheless, in spite of the study of pyrene-based CMPs for iodine adsorption, the adsorption capacity is not high.^{14,18,19} In the last few years, the built blocks used in CMPs are most 1,3,6,8-tetrasubstituted pyrene,⁹⁻²⁸ but there are a few 1,3,6,8-tetrasubstituted pyrene-based CMPs used as fluorescent sensing materials,^{15-17,20-28} as well as a small amount of 2,7-disubstituted,¹⁵ 1,3-disubstituted pyrene.²⁹ To the best of our knowledge, the CMPs containing 1,6-disubstituted pyrene have not been reported yet. Because the asymmetric structure of the 1,6-disubstituted pyrene can increase the free volume, prevent the fluorescence quenching caused by stacking, we speculate that the CMPs containing 1,6-disubstituted pyrene should possess excellent adsorptive and fluorescent sensing properties.



Scheme 1. Synthesis of the TDP, PCPP, TTPDP, and TDTPAP.

^a Anhui Province Key Laboratory of Optoelectronic and Magnetism Functional Materials; School of Chemistry and Chemical Engineering, Anqing Normal University, Anqing 246011.

† Electronic Supplementary Information (ESI) available: Synthesis of three monomers, FT-IR, PXRD, TGA, UV-Vis, SEM, HOMO-LUMO energy levels, and Raman spectra of the four CMPs, Recycling percentage, Effects of solvents, response time, and NACs on fluorescent spectra. See DOI:10.1039/x0xx00000x

In this context, we report the synthesis and characterization of four 1,6-disubstituted pyrene-based CMPs. They were synthesized by Sonogashira–Hagihara reaction (TDP), trimerization reaction of bi-cyano compound (CPP) catalyzed with trifluoromethanesulfonic acid (PCPP), and Friedel-Crafts reaction catalyzed with $\text{CH}_3\text{SO}_3\text{H}$ (TTPDP and TDTPAP), respectively (Scheme 1). Their performance of adsorbing and fluorescence sensing to iodine have been comparatively studied.

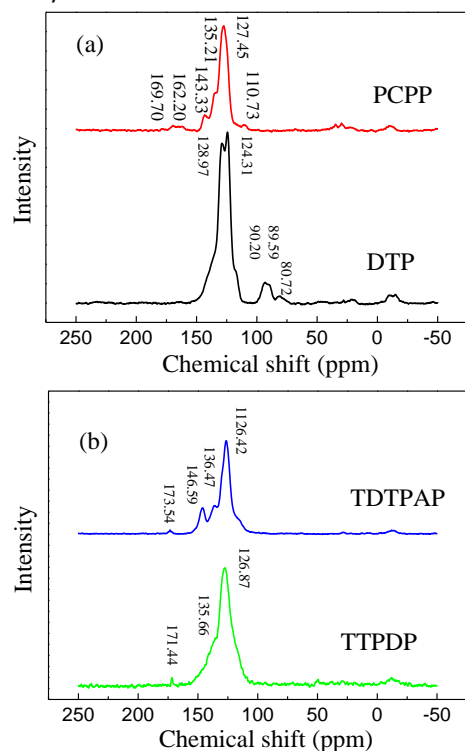


Fig. 1. The $ss^{13}\text{C}$ NMR spectra of the four CMPs.

Experimental

3 mmol of 1,6-dibromopyrene, 0.159 mmol of CuI , 3 mmol of 1,3,5-triethynylbenzene (TEB), and 0.0516 mmol of Tetrakis(triphenylphosphine) palladium ($\text{Pd}(\text{PPh}_3)_4$) were placed in a round-bottom flask with a magnetic stirring rod and a reflux condenser. The solids were dissolved in a mixture of N,N -dimethylformamide (DMF) (12 mL) and anhydrous triethylamine (TEA) (12 mL). After degassing the mixture for 30 min, the reaction was carried out at 90°C for 3d under a nitrogen atmosphere with stirring. We cooled the mixture for a while and eventually reached normal room temperature. The brown powder was collected by filtration and they are washed four times with chloroform, water, methanol and acetone (25 mL \times 4) for each to remove any catalyst or unreacted substance. Then, the powder was further washed with methanol, chloroform and tetrahydrofuran (THF) for 24 h using a Soxhlet extractor. Ultimately, the product was dried at 50°C under vacuum for 24 h to afford brown powder (Abbreviation as TDP) to (95 %). FTIR (cm^{-1}): 3447, 2192, 1628, 1574, 1383, 872, 840. Solid state CP/MAS ^{13}C NMR ($ss^{13}\text{C}$ NMR) of TDP (chemical

shift: ppm): 82, 90, 124, 129. Theoretical: C, 96.19; H, 3.81. Found: C, 93.67; H, 4.335. DOI: 10.1039/C9NJ05509F

Trifluoromethanesulfonic acid ($\text{CF}_3\text{SO}_3\text{H}$, 3.04 mL, 23.16 mmol) and 30 mL of anhydrous CHCl_3 was charged into a pre-dried 3-neck round bottom flask under N_2 atmosphere. The mixture was cooled to 0°C , and the solution of CPP (1.4302 mmol) and CHCl_3 (60 mL) was dropwisely added into the mixture over 30 min. The mixture was stirred at 0°C for 2 h, and then left overnight at 40°C , which was poured into 100 mL of water containing 12 mL of ammonia solution and stirred for another 2 h. The solid precipitate was filtered and washed with water, chloroform and then extracted Soxhlet extractor with chloroform, methanol, and acetone, successively. The product was dried in vacuum at 50°C for 24 h to give brown-yellow powder (yield: 73.80 %). FT-IR (KBr, cm^{-1}): 1670, 1606, 1502, 1390, 1315, 1182, 1004, 845, 815. $ss^{13}\text{C}$ NMR (δ : ppm): 170–162; 143, 135; 127, 111. Theoretical: C 89.086, N 6.926; H 3.987. Found: C 88.31, N 7.656, H 4.031.

2,4,6-Trichloro-1,3,5-triazine (TCT) (1.6 mmol) and TPDP (1.2 mmol) were dissolved in 12 mL of dry o -dichlorobenzene, $\text{CH}_3\text{SO}_3\text{H}$ (16.8 mmol) was added the solution, then heated at 140°C for 48 hours. The precipitate was filtered off from the hot reaction mixture was soxhlet extracted overnight with methanol, THF and acetone and dried in vacuum. The target product (TTPDP) was obtained as a black colored solid with yield of 84.85 %. FT-IR (KBr, cm^{-1}): 343, 1622, 1595, 1564, 1473, 1383, 813, 749. $ss^{13}\text{C}$ NMR: 127, 136, 171. Theoretical calcd.: C 82.48, H 4.40, N 13.12. Found: C 79.92, H 4.575, N 11.088.

TDTPAP was obtained as brownish red colored powder using the same procedures (yield: 82.17 %). FTIR (KBr, cm^{-1}): 3421, 1628, 1542, 1468, 1383, 797, 697. $ss^{13}\text{C}$ NMR (ppm): 112, 136, 147, 174. Anal. calcd.: C 84.83, N 10.06, H 4.58. Found: C 80.25, N 8.186, H 4.975.

Results and discussion

The efficient synthesis and characterization of the monomers CPP, TPDP, and DTPAP were seen in S3-S5 and Fig. S1-S6. The synthesis routes for the four CMPs with 1,6-disubstituted pyrene as core are displayed in Scheme 1. TDP was directly synthesized through Sonogashira–Hagihara coupling reaction catalyzed by palladium and using a 1.5:1 molar ratio of ethynyl to bromo functionalities, since this was found to maximize surface areas in the CMPs. Moreover, DMF as a solvent might give rise to higher surface area materials.³⁰ CPP with 1,6-disubstituted pyrene and two aromatic nitriles was selected as the precursor for the synthesis of PCPP.³¹ The $\text{CF}_3\text{SO}_3\text{H}$ rather than zinc chloride was applied to catalyze the cross-linking trimerization reaction at a much lower temperature (40°C) for a shorter time,^{32,33} which offers a significant advantage, avoiding many undesired decomposition and condensation reactions such as C-H bond cleavage and carbonization,³⁴ as well as avoid remaining metallic species. After extensive washing, the insoluble polymer was collected as fine powders in colors form brown-yellow with a yield about 73.80 %.³¹

Unlike the black materials obtained via ionothermal synthesis, the polymer received after TFMSA catalyzed condensation is fluorescent powder. TTPDP and TDTPAP were prepared by a Friedel–Crafts reaction of TCT with TPDP and DTPAP with $\text{CH}_3\text{SO}_3\text{H}$ as a catalyst, which were well-defined para-substituted inferred via the model product, simple and convenient, including moderate processing temperature, the inexpensive catalysts relatively low toxicity, and commercially available TCT and the building blocks without special functional groups are used, preferably in a metal-free regime.³⁵

Their structures were characterized by Fourier transform infrared (FT-IR) spectroscopy. In Fig. S7a, the characteristic terminal $\text{C}\equiv\text{C}-\text{H}$ triple bond vibration peaks at about 3298 cm^{-1} had very lower intensity for TDP, while the peaks at around 2192 cm^{-1} , which were characteristic of substituted acetylene, were easily detected.³⁶ The strong absorption peak situated at 840 cm^{-1} was assigned to the substituted phenylene, while the absorb summits at circa 1628, 1574, and 1383 cm^{-1} belonged to the benzene and pyrene.³⁷ The spectra of PCPP in Fig. S7b show significant decrease in the intense of carbonitrile band around at 2228 cm^{-1} along with the emergence of strong peaks of triazine rings at 1502, 1390, and 800 cm^{-1} , indicative a high degree of reaction.^{31,32,34} Fig. S7cd show the FT-IR spectra of the TTPDP and TDTPAP networks. The stretching vibration summit of C-Cl located at 847 cm^{-1} almost disappears, indicating the complete conversion of C-Cl.³⁵ The emerging of the absorption bands at 1602, 1563, and 1468 cm^{-1} prove the existence of the triazine ring (Fig. S7bcd). In Fig. S7, the characteristic peaks at 1574, 1606, 1595, 1542 and 1383, 1390, 1380, 1383 cm^{-1} should be put down to benzene ring. Further evidence of the formation of the target networks are given by the intense bands at 1627, 1670, 1622 and 1628 cm^{-1} , which are attributed to pyrene ring.^{36,37} The CMPs were further characterised at the molecular level by ss ^{13}C NMR. As shown in Fig. 1, the peaks at around 174–162 ppm are from the C=N in the s-triazine rings.³¹⁻³⁴ The signal at 143 ppm belongs to the carbon atom of the phenyl or pyrene ring connecting the triazine ring and pyrene ring or phenyl ring. The peak at 135 ppm is assigned to the carbon in pyrene. Wide peak center at 127 ppm correspond to the unsubstituted phenyl and pyrene carbon.^{31,33} The low intensity peaks at 111–110 ppm are ascribed to the SP carbon from residual -CN.³¹⁻³⁴ Elemental analysis of forementioned CMPs show some deviations common for microporous materials due to incomplete combustion and adsorbed water and gases in the pore structure.^{31,34} UV-Vis absorption spectra were used to compare the electronic properties of the CMPs against the starting materials (Fig. S8). The broad absorption between 200 and 800 nm observed in the four CMPs are the result of complementary absorption of the pyrene-based building block. The absorption of the pyrene moiety were shifted from 385, 267/357, 537, and 429 nm for the four micropore materials (TDP, PCPP, TTPDP, as well as TDTPAP) to 464, 411/561, 598, and 535 nm in relative monomers. These results indicate the extended conjugation in the CMPs.^{13,14,16,20}

The CMP networks were insoluble in organic solvents and various aqueous conditions, implying their good chemical stability. Thermogravimetric analysis (TGA) revealed that the decomposition temperature of the CMPs in nitrogen are 140, 352/581, 350/563, and $573\text{ }^\circ\text{C}$, respectively (Fig. S9).^{31,34} Powder X-ray diffraction measurements (XRD) (Fig.S10) showed that the CMP networks were amorphous, and no evidence for characteristic reflections from a crystalline phase or layered sheets was observed. SEM images showed that TDP shows a series of aggregated particles, while other three CMPs are made up of blocks. (Fig. S11).³⁸

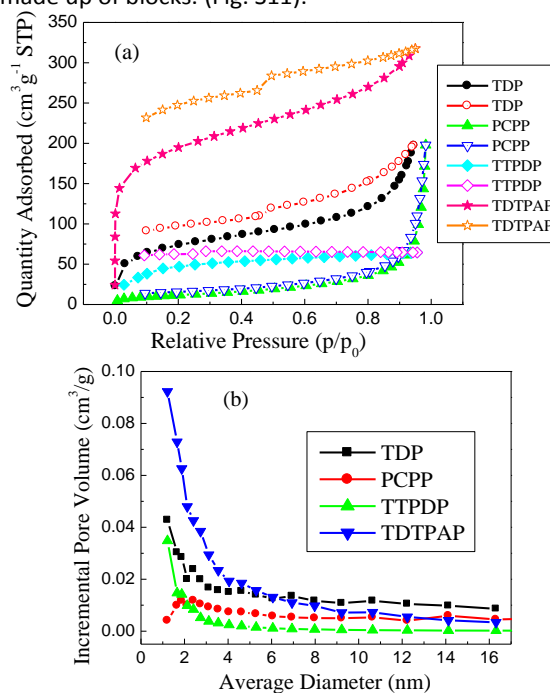


Fig. 2. (a) Nitrogen adsorption-desorption isotherms measured at 77 K for ● TDP, ▲ PCPP, ◆ TTPDP, and ★ TDTPAP; (b) BJH pore size distribution profile of TDP, PCPP, TTPDP, and TDTPAP. ●▲◆★ Adsorption isothermal curves, ○△◇☆ Desorption isothermal curves.

Porosity of the resulting CMPs were studied by means of nitrogen adsorption–desorption measurement at 77.3 K (Fig. 2). TDP, PCPP, TTPDP, and TDTPAP perform Type II, Type III, Type I, and Type II gas sorption isotherms as well as some hysteresis phenomenon, which might be attributed to the existence of a mesoporous structure and interparticulate voids of the samples.^{31,33,34} The four CMPs showed a significant low-pressure hysteresis, which are diffusional limitations by pore blocking influences arised as a consequence of the micropore morphology and connectivity rather than swelling effects.³⁹ If low pressure adsorption-desorption isotherms would have been recorded, there would not be a closure of the isotherms. This behavior was associated with the irreversible uptake of gas molecules in the pores (or through pore entrances).⁴⁰ Pore size distribution curves for the CMPs calculated using nonlocal density functional theory (NL-DFT) are shown in Fig. 2b. The polymer networks exhibited the micropore diameter centering around 1.22, 1.22, 1.88, and 1.22 nm, respectively, in agreement with the shape of the N_2 isotherms (Fig. 2a).³⁴ As

shown in Table 1, PCPP has the lowest apparent BET surface area with $43.0 \text{ m}^2 \text{ g}^{-1}$, whereas other CMPs possess not only high apparent BET surface areas (261.9 , 187.5 , and $695.2 \text{ m}^2 \text{ g}^{-1}$ for TDP, TTPDP, and TDTPAP, respectively), but also large micropore volume at $p/p_0=0.1$ ($V_{0.1}$) with 0.23 , 0.30 , 0.049 , and $0.26 \text{ cm}^3 \text{ g}^{-1}$. In accordance with calculating from single point measurements ($p/p_0=0.97$), the pore volumes are 0.31 , 0.30 , 0.10 , and $0.49 \text{ cm}^3 \text{ g}^{-1}$.^{31,34} The $V_{0.1}/V_{\text{tot}}$ value which is the micropore volume divided by the total pore volume gives an indication of the percentage microporosity in the materials, which are higher than 0.40 (Table 1), meaning that micropores are dominant in the networks. Their highly rigid and contorted molecular structure based on the conatural structure of 1,6-disubstituted pyrene should prohibit space-efficient packing in the solid state.^{31,32}

Table 1. Pore and surface properties of CMPs.

CMPs	S_{BET}^a ($\text{m}^2 \text{ g}^{-1}$)	S_{Langmuir}^a ($\text{m}^2 \text{ g}^{-1}$)	V_{total}^b ($\text{cm}^3 \text{ g}^{-1}$)	V_{micro}^c ($\text{cm}^3 \text{ g}^{-1}$)	$V_{\text{micro}}/V_{\text{total}}$	S_{micro}^c ($\text{m}^2 \text{ g}^{-1}$)
TDP	261.9	-	0.3051	0.2292	0.7512	123.9
PCPP	43.0	51.8	0.3036	0.2977	0.9729	4.3
TTPAP	187.5	-	0.0999	0.0493	0.4932	56.6
TDTPAP	695.2	-	0.4913	0.2659	0.5412	214.6

^a Specific surface area calculated from the adsorption branch of the nitrogen isotherm using the BET method in the relative pressure (p/p_0) range from 0.01 to 0.10 .

^b Total pore volume is obtained from BET data up to $p/p_0=0.99$ and is defined as the sum of micropore volume and volumes of larger pores.

^c Micropore volume calculated from nitrogen adsorption isotherm using the t plot method.

Recently, the development of porous absorbents for efficient I_2 capture has attracted considerable attention because I_2 is a dangerous radioisotope in nuclear waste, such as ^{129}I , which is an important radioisotope in nuclear waste with a very long half-life of 1.57×10^7 years.^{40,41} The I_2 capture was conducted under typical fuel reprocessing conditions (350 K and ambient pressure, the as-loaded materials are denoted as $\text{I}_2\text{@CMPs}$). For each measurement, the dried CMP powder was placed in a pre-weighted glass vial. The vial and excess solid iodine were put together in a closed system at ambient pressure and 350 K .⁴¹⁻⁴³ As time progressed, the color of TDP, PCPP, and TDTPAP changed from russetish, brown yellow, and brown to almost black (Fig. S12).⁴¹⁻⁴⁵ Due to the color of TTPDP is deep black, hence, the color change of the sample could not be found with the time progressed. Fig. 3 shows the weight of the samples at various time intervals during the iodine uptake. The iodine adsorption increased significantly with prolonged contact time. In the initial 12 h , the adsorption capacities of CMPs were relatively quick. No further change in the iodine loading amounts was observed after 48 h , suggesting that the systems were basically saturated. The equilibrium iodine uptakes of TDP, PCPP, TTPDP, and TDTPAP were 0.61 , 3.07 , 3.49 , 4.19 g g^{-1} .⁴¹⁻⁴⁵ The iodine adsorption capacity of TTPDP and TDTPAP are the highest values in that of the pyrene-based POPs (Table S1) and are comparable to that of triazine-based POPs and triphenylamine-based POPs (Table S2). It can be seen

that the adsorptive capacity of PCPP, TTPDP, and TDTPAP are higher than that of TDP, which indicated that s-triazine ring plays a vital role in increasing iodine capture, because introducing of the electron-deficient s-triazine may enhance the dipole-dipole interaction between sorbate molecule and adsorbent.⁴⁶ In addition, there was only the nonpolar interaction of π -surfaces of triple bonds and pyrene with I_2 rather than chemical bond formation between I_2 and acetylene bonds.¹⁸ As shown in Fig. S7 and Table S3, the center or intensity of the peaks of pyrene and benzene units have more changes after introducing triazine. Moreover, the iodine adsorption capacity of TTPDP and TDTPAP are greater than that of PCPP, which means that the triphenylamine (TPA) units can enhance the iodine adsorption ability. This is because TPA are provided with electron-rich, propellerlike geometry, and central electroactive nitrogen atom.⁴⁷ These results are of great significance for the design iodine adsorbed porous organic polymers. TGA was also conducted on $\text{I}_2\text{@CMPs}$ to calculate the I_2 loading (Fig. S9). The TGA curves revealed the significant weight loss of the iodine-loaded CMPs in the range of 90 to $350 \text{ }^\circ\text{C}$. The mass loss of iodine were thus estimated to be 0.53 (86.43%), 2.66 (86.54%), 3.32 (95.15%), and 3.86 (92.12%) g g^{-1} relative to the mass of TDP, PCPP, TTPDP, and TDTPAP.^{48,49} The subtle differences may be caused by some incomplete release of iodine at the calculated temperature.⁵⁰

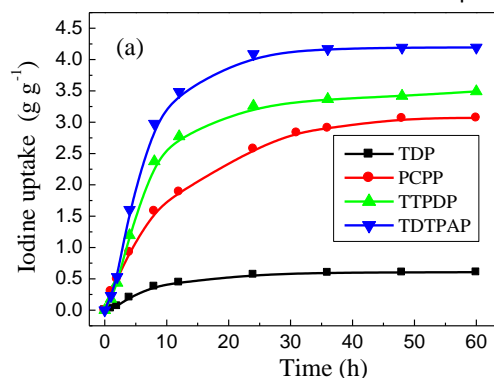


Fig. 3. Gravimetric uptake of iodine as a function of time at 350 K .

The adsorption selectivity has been carried out with water, cyclohexane (CHA), ethanol (EtOH), and dioxane (DOX) at 350 K for 60 h (Fig. 4). The uptake capacity of TDP, TTPDP, and TDTPAP decreased with the increase of a solvent's polarity. Delightedly, the water sorption values of the three CMPs are very low, which leads to a high iodine–water selectivity. Therefore, TDP, TTPDP, and TDTPAP could sorption iodine over water which is advantageous for the actual industrial application of the iodine sorption process under humid condition.⁴⁵

The strong interactions expected to exist between the π -electron systems and iodine in the CMPs could be considered using modern analytical instruments. The UV-Vis spectra of $\text{I}_2\text{@CMPs}$ (Fig. S13) showed that no additional peaks at about 731 nm resulting from pristine iodine crystals were observed in the iodine-loaded sorbents. Moreover, powder XRD measurement (Fig. S14) revealed that $\text{I}_2\text{@CMPs}$ were amorphous in nature without any prominent crystalline

diffraction peaks, indicating that the adsorbed iodine molecules were completely transformed into polyiodide anions.⁵¹ The structure of the iodine inside the pores of the CMPs were revealed by Raman spectroscopy (Fig. S15). The strong peak located at about 165 cm^{-1} belonged to I_5^- . The laboratorial results indicate that the charge transfer occurred between the guest iodine molecules and the electron-rich host networks at high extent.^{44,52}

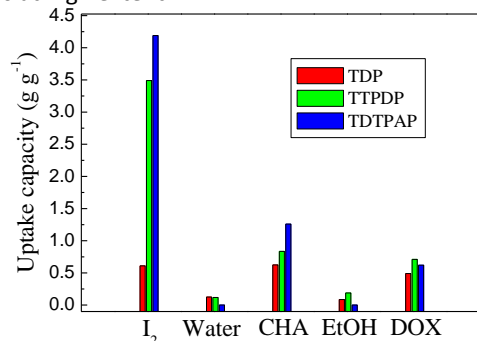


Fig. 4. The adsorption selectivity of TDP, TTPDP, and TDTPAP for I_2 , water, CHA, EtOH, and DOX.

When the I_2 -loaded TDP, PCPP, TTPDP, and TDTPAP were heated at 398 K under ambient pressure and air atmosphere for 120 min, iodine release efficiency was as high as 99.72 %, 95.21 %, 97.13 %, and 96.26 % (Fig. S16).^{44,51} The excellent iodine release encouraged us to exploit the recyclability of the adsorbents. Recycling was performed by taking iodine-loaded PCPP, TTPDP, and TDTPAP samples (after exposure of as-synthesized CMPs to iodine for 24 h at 350 K) and heating at 398 K for 120 min. The samples were then reused for iodine uptake again at same conditions. After reusing three times, the iodine uptake percentage of PCPP, TTPDP, and TDTPAP were 93.06 %, 95.88 %, and 88.65 %, while recycling percentage were found to be 95.89 %, 86.52 %, and 91.51 %, respectively (Fig. S17). These very high values make our CMPs to be attractive materials for use as the robust recyclable and reversible iodine adsorbents.^{51,53}

In addition, the CMPs are capable of trapping iodine in solution. To estimate the adsorption kinetics of CMPs for iodine-CHA solution, the UV-Vis spectra were employed to measure the change of the maximum adsorption at 523 nm (Fig. S18 and S19). It can be seen that two stages of adsorption kinetic were obtained: the adsorption capacity for iodine increased quickly during the first 12, 12, 1, and 12 h for TDP, PCPP, TTPDP, and TDTPAP, respectively, and after these the slow increases were observed until equilibrium were reached. Removal efficiency of PCPP and TTPDP with 86.80 % and 99.92 % were acquired for iodine solutions in 300 mg L^{-1} , while removal efficiency of TDP and TDTPAP with 87.71 % and 90.91 % were achieved in iodine solutions of 100 mg L^{-1} .^{40,42,44} Furthermore, the colors of the solution of iodine in cyclohexane became paler, which indicated that the iodine was encapsulated into the CMP networks to successively generate $I_2@CMPs$.⁵³ It is important to note that the adsorption rate of TTPDP is the fastest and the removal efficiency is the highest. Even in iodine

solutions of 300 mg L^{-1} , the adsorption equilibrium only need 1 hour, and the removal efficiency of 99.92% was obtained.

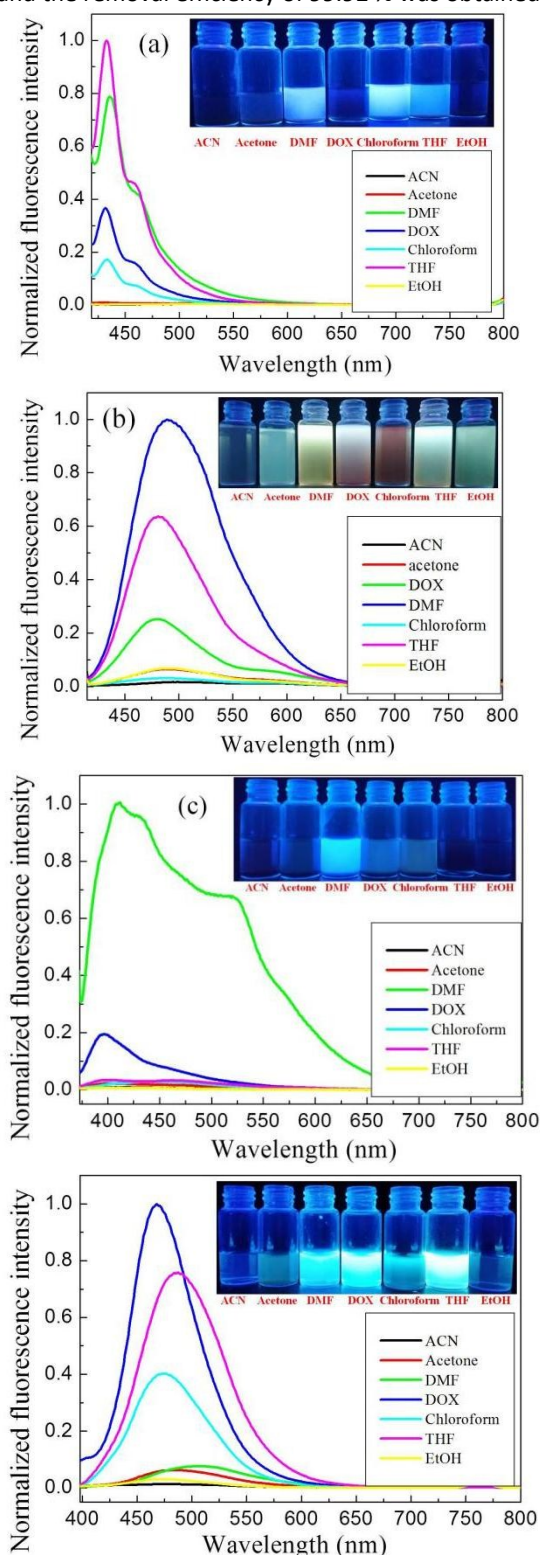


Fig. 5. Fluorescence spectra of CMPs dispersed in different solvents [(a)TDP: $\lambda_{\text{ex}}=400\text{ nm}$, (b) PCPP: $\lambda_{\text{ex}}=400\text{ nm}$, (c) TTPDP: $\lambda_{\text{ex}}=350\text{ nm}$, (d) TDTPAP: $\lambda_{\text{ex}}=380\text{ nm}$]. Inserts: The fluorescence photographs of CMPs dispersed in different solvents, where fluorescence is excited under 365 nm using a portable UV lamp.

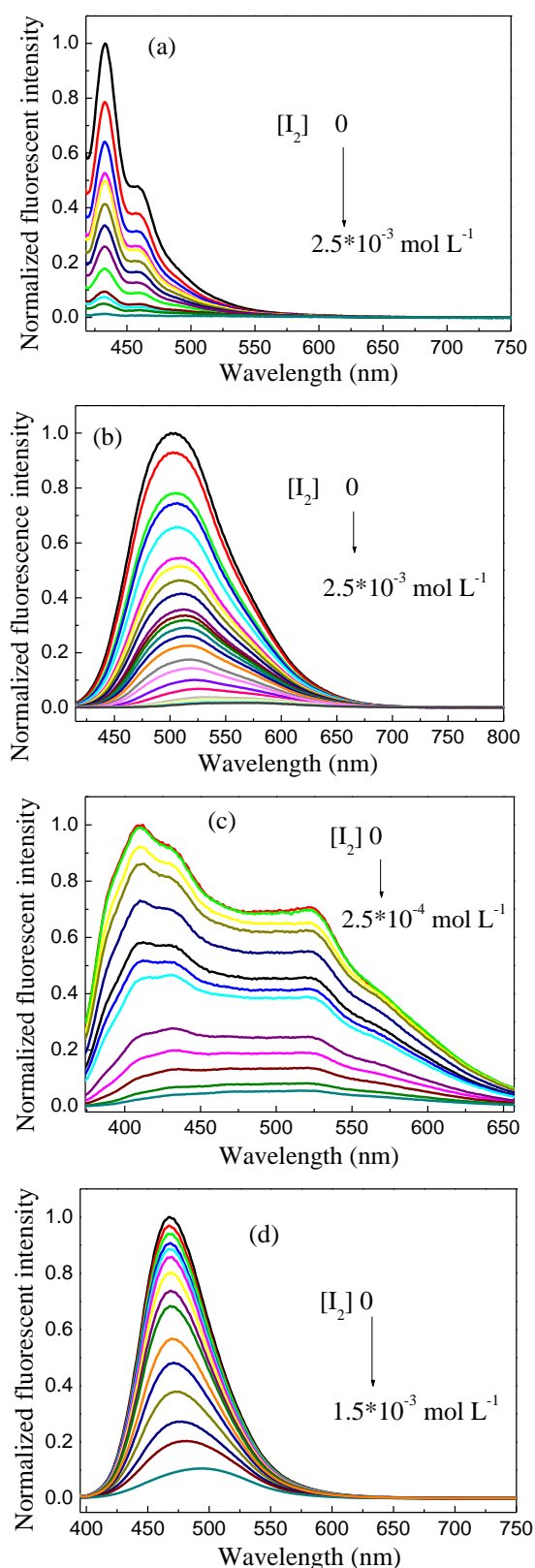


Fig. 6. Fluorescence spectral changes of (a) TDP ($\lambda_{\text{ex}}=400 \text{ nm}$, in DMF), (b) PCPP ($\lambda_{\text{ex}}=400 \text{ nm}$, in DMF), (c) TTPDP ($\lambda_{\text{ex}}=350 \text{ nm}$, in DMF), and (d) TDTPAP ($\lambda_{\text{ex}}=380 \text{ nm}$, in DOX) upon addition of I_2 .

The encapsulated iodine could be readily eliminated from the frameworks upon immersion of I_2 @CMPs in organic solvents. The iodine-loaded CMPs were soaked in fresh ethanol, the color of the ethanol solution deepened from colorless to dark brown, which clearly indicates that the guests are dissociated from the CMP frameworks (Fig. S20 and S21 Inserts).⁴³ To investigate the kinetics of iodine delivery by CMPs, the UV-Vis spectra were recorded at room temperature. The iodine release rates become slower after 8, 4, 8, and 4 h owing to the fact that the concentration of iodine in ethanol increased with time. After 12 h, however, about 75.14 %, 84.82 %, 55.47%, and 64.10 % of the initial iodine had been released from I_2 @CMPs, indicating the reversibility of the iodine adsorption process.^{41,51}

The TDP, PCPP, TTPDP, and TDTPAP possess high absolute fluorescence quantum yields with 78.32 %, 63.45 %, 51.57 %, and 70.45 %, which encouraged us to explore their fluorescence sensing properties for iodine. The four CMPs were dispersed in common organic solvents, such as ACN, acetone, DMF, DOX, chloroform, THF, and EtOH. As shown in Fig. 5, their fluorescence spectra showed remarkable differences.^{54,55} Among these solvents, the most explicit fluorescence enhancement in THF, DMF, DOX to CMPs, and low emission were observed in ACN, EtOH, and acetone.⁵⁵⁻⁵⁷ Another interesting phenomenon was observed, upon exciting under the UV light at 365 nm, TDP transmits blue fluorescence in the dispersions of DMF, chloroform, and THF. PCPP emitted various colored fluorescence in the dispersions of these solvents except for ACN. TTPDP emitted blue fluorescence only in the dispersion of DMF. TDTPAP emitted bright cyan fluorescence in the dispersions of DMF, DOX, and THF (Fig. 5. Inserts).^{56,57} The sensing performance of CMPs to I_2 solution has been reported. When I_2 was added into the dispersion of the CMPs (Fig. S22), we observed that the fluorescence emission was almost instantaneously reduced.^{58,59} These results indicated that the microporous architecture facilitates the sensing process and improves the response to NACs and I_2 .⁶⁰

When quantitative I_2 was added into the 1.0 mg mL^{-1} of the four CMPs dispersions, respectively, it was found that fluorescence of the dispersions could be readily quenched by I_2 (Fig. 6).^{16,31} Obviously, the fluorescence quenching degrees of the four CMPs in various solvents were different.^{15,17,54} We further use the Stern-Volmer equation to calculate the quenching coefficients: $I_0/I = 1 + K_{\text{sv}}[I_2]$,¹² where I is the fluorescence intensity after adding the I_2 of concentration, and K_{sv} is the quenching coefficient. There are good linear Stern-Volmer relationships of the four CMPs for sensing to I_2 . Delightfully, the K_{sv} and limits of detection (LOD) of the four CMPs reach from 10^3 to 10^5 L mol^{-1} and from 10^{-13} to $10^{-9} \text{ mol L}^{-1}$, respectively (Fig. S23 and Table S4).^{15,16,31,54,55} To the best of our knowledge, PCPP is one of the highest sensitivities for fluorescence sensing to iodine (Table S5).⁶⁰ Although the TPA units can improve the adsorption performance of iodine, the improvement of the sensing performance is not significant.⁶¹ The order of sensitivity of fluorescence sensing to iodine is: PCPP(1.40×10^5) > TDP(6.10×10^4) > TTPDP(2.02×10^4) > TDTPAP

(4.65×10^3). This result means that the distorted structure of 1,6-pyrene is enough to prevent the fluorescence quenching caused by pyrene aggregation. The introduction of the TPA units into the CMP networks can reduce their sensitivity to iodine.

To better study the effects of nitroaromatic compounds (NACs), such as *o*-nitrophenol (*o*-NP), PA, 2,4-dinitrotoluene (DNT), nitrobenzene (NB), *m*-dinitrobenzene (*m*-DNB), *p*-dinitrobenzene (*p*-DNB), *p*-nitrotoluene (NT), as well as phenol (PhOH), *o*-dichlorobenzene (DCIB) on the sensing property of TDP, TTPDP, and TDTPAP for I_2 , we performed a series of selectivity and competition experiments by testing the fluorescence changes in the presence of I_2 . It can be seen from Fig. S24 (red bars) that TDP and TTPDP have high selectivity for I_2 , the PCPP has high selectivity for PA, and TDTPAP has high selectivity for I_2 and *o*-NP.^{15,54} The introduction of the TPA units into the CMP networks can reduce their selectivity to iodine. The competition of CMPs toward the I_2 or PA detection were then investigated by testing the fluorescence change in the presence of CMPs (1.0 mg mL^{-1}) and I_2 or PA adding equal equivalent of other NACs and I_2 . It showed that the fluorescent intensity of PCPP almost has no appreciable influence on PA after added NACs, while the fluorescent intensity of TDP, TTPDP, and TDTPAP almost has also no obvious influence on I_2 after added NACs except for PA and *o*-NP.¹⁵

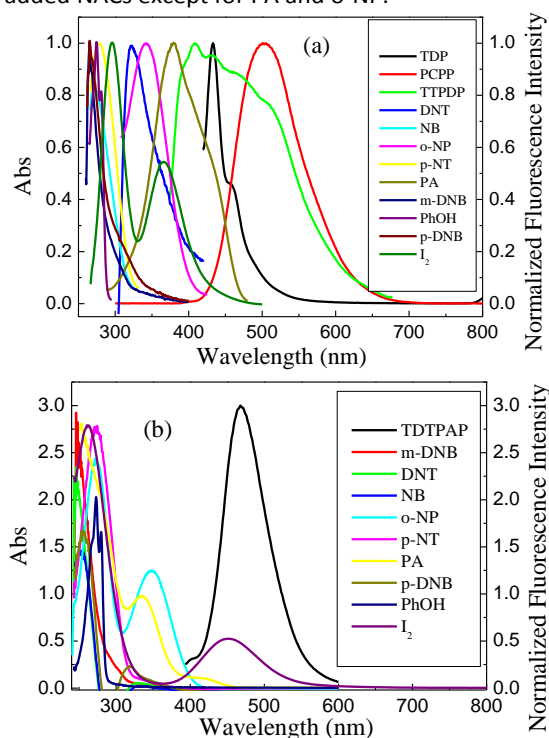


Fig. 7. The absorption spectra of I_2 and NACs (*o*-NP, PA, PhOH, DNT, *p*-NT, *m*-DNB, *p*-DNB, and NB) and fluorescence spectra of (a) TDP ($\lambda_{\text{ex}}=400 \text{ nm}$), PCPP ($\lambda_{\text{ex}}=400 \text{ nm}$) and TTPDP ($\lambda_{\text{ex}}=350 \text{ nm}$) in DMF; (b) TDTPAP ($\lambda_{\text{ex}}=380 \text{ nm}$) in DOX (1.0 mg mL^{-1}).

We also investigated the adsorbing and quenching mechanism by measuring the absorption spectra of I_2 , NACs (*o*-NP, PA, PhOH, DNT, *p*-NT, *p*-DNB, *m*-DNB, and NB), PhOH, DCIB, and made a comparison with the emission spectra of the

four CMPs. As shown in Fig. 7, there are overlaps between the two spectra of PA and the four CMPs, as well as between the spectra of I_2 with the TDP, TTPDP, and TDTPAP, which means that there are energy transfer between PA, I_2 and some CMPs, suggesting that they are the both energy transfer mechanism and electrons transfer mechanism.¹⁵ The calculated the lowest-unoccupied molecular orbital (LUMO) energy level of I_2 is -4.988 eV , which is much lower than that of the four CMPs (TDP: -2.224 , PCPP: -2.062 , TTPDP: -2.026 , and TDTPAP: -2.060 eV), thus providing a strong driving force for the electron transfer (Table 2 and Fig. S25). Upon excitation, electrons are transferred from the conduction band of CMPs to the LUMO of the I_2 , which result in the formation of complex of polyiodide anion and CMP skeleton, leading to the quenching and adsorption phenomenon.⁶¹ In addition, the of electrovalent bonds between polyiodide anion and CMP skeleton, as well as the hydrogen bonds of PA, *o*-NP and CMP networks can also greatly enhance adsorption and fluorescence sensing.^{28,62}

Table 2. HOMO and LUMO calculations for the four CMPs, I_2 and the NCAs. All the molecular orbital calculations were performed with the Gaussian 09 D 0.1 program at the B3LYP/6-31G* level.

MO energy (eV)	TDP	PCPP	TTPDP	TDTPAP	I_2
LUMO	-2.224	-2.062	-2.026	-2.060	-4.988
HOMO	-5.114	-5.278	-5.311	-5.271	-7.553
MO energy (eV)	<i>p</i> -NT	DNT	NB	<i>p</i> -DNB	<i>m</i> -DNB
LUMO	-2.318	-2.977	-2.428	-3.495	-3.135
HOMO	-7.364	-8.1131	-7.591	-8.350	-8.413
MO energy (eV)	PA	<i>o</i> -NP	PhOH		
LUMO	-3.898	-2.711	-0.3331		
HOMO	-8.237	-6.797	-6.566		

Conclusions

In conclusion, four 1,6-disubstituted pyrene-based fluorescent conjugated microporous polymers with amorphous structure were successfully designed and synthesized by different polymerization reactions, such as a Sonogashira–Hagihara polycondensation reaction (TDP), trimerization reaction of bi-cyano compound catalyzed using trifluoromethanesulfonic acid (PCPP), and Friedel-Crafts reaction catalyzed by $\text{CH}_3\text{SO}_3\text{H}$ (TTPDP and TDTPAP). The performance of adsorb and fluorescence sensing to iodine for the four CMPs have been comparatively studied. It is found that the four CMPs display reversible guest uptake in iodine vapor. The four CMPs exhibit high sensitivity to iodine via fluorescence quenching. In especial, PCPP exhibited extremely high detection sensitivity to I_2 . To the best of our knowledge, it displays the highest reported K_{SV} value and lowest detection limit to iodine to date. Although the introduction of the TPA units into the CMP networks can improve the adsorption performance of iodine, it can reduce their fluorescence sensing sensitivity and selectivity to iodine.

Acknowledgements

This work was supported by Natural Science Foundation of Anhui Education Department (under Grant No. KJ2018A0319).

References

- 1 X. Feng, X. S. Ding, D. L. Jiang, *Chem. Soc. Rev.*, 2012, **41**, 6010–6022.
- 2 N. B. McKeown, B. Gahnem, K. J. Msayib, P. M. Budd, C. E. Tattershall, K. Mahmood, S. Tan, D. Book, H. W. Langmi, *Angew. Chem. Int. Ed.*, 2006, **45**, 1804–1807.
- 3 D. Yuan, W. Lu, D. Zhao and H. C. Zhou, *Adv. Mater.*, 2011, **23**, 3723–3725.
- 4 Z. A. Qiao, S. H. Chai, K. Nelson, Z. H. Bi, J. H. Chen, S. M. Mahurin, X. Zhu, S. Dai, *Nat. Commun.*, 2014, **5**, 3705.
- 5 Z. H. Li, D. C. Wu, Y. R. Liang, R. W. Fu, K. Matyjaszewski, *J. Am. Chem. Soc.*, 2014, **136**, 4805–4808.
- 6 M. J. Bojdys, J. Jeromenok, A. Thomas, M. Antonietti, *Adv. Mater.*, 2010, **22**, 2202–2205.
- 7 J. W. Colson, A. R. Woll, A. Mukherjee, M. P. Levendorf, E. L. Spitler, V. B. Shields, M. G. Spencer, J. Park, W. R. Dichtel, *Science*, 2011, **332**, 228.
- 8 X. Liu, Y. Xu, D. Jiang, *J. Am. Chem. Soc.*, 2012, **134**, 8738–8741.
- 9 J. X. Jiang, A. Trewin, D. J. Adams, A. I. Cooper, *Chem. Sci.*, 2011, **2**, 1777–1781.
- 10 K. V. Rao, S. Mohapatra, T. K. Maji, S. J. George, *Chem. Eur. J.*, 2012, **18**, 4505–4509.
- 11 Z. J. Yan, H. Ren, H. P. Ma, R. R. Yuan, Y. Yuan, Xi. Q. Zou, F. X. Sun, G. S. Zhu, *Micropor. Mesopor. Mat.*, 2013, **173**, 92–98.
- 12 M. Yu, X. Y. Wang, X. Yang, Y. Zhao, J. X. Jiang, *Polym. Chem.*, 2015, **6**, 3217–3223.
- 13 R. S. Sprick, J. X. Jiang, B. Bonillo, S. J. Ren, T. Ratvijitvech, P. Guignon, M. A. Zwiijnenburg, D. J. Adams, A. I. Cooper, *J. Am. Chem. Soc.*, 2015, **137**, 3265–3270.
- 14 K. C. Park, J. Cho, C. Y. Lee, *RSC Adv.*, 2016, **6**, 75478–75481.
- 15 L. Guo, D. P. Cao, J. Yun, X. F. Zeng, *Sensor. Actuat. B–Chem.*, 2017, **243**, 753–760.
- 16 D. X. Wang, S. Y. Feng, H. Z. Liu, *Chem. Eur. J.*, 2016, **22**, 14319–14327.
- 17 G. Q. Lin, H. M. Ding, D. Q. Yuan, B. S. Wang, C. Wang, *J. Am. Chem. Soc.*, 2016, **138**, 3302–3305.
- 18 D. Shetty, J. Raya, D. S. Han, Z. Asfari, J. C. Olsen, A. Trabolsi, *Chem. Mater.*, 2017, **21**, 8968–8972.
- 19 G. Das, T. Skorjanc, S. K. Sharma, T. Prakasam, C. Platas-Iglesias, D. S. Han, J. Raya, J. C. Olsen, R. Jagannathan, A. Trabolsi, *ChemNanoMat.*, 2018, **4**, 61–65.
- 20 M. A. Zwiijnenburg, G. Cheng, T. O. McDonald, K. E. Jelfs, J. X. Jiang, S. J. Ren, T. Hasell, F. Blanc, A. I. Cooper, D. J. Adams, *Macromolecules*, 2013, **46**, 7696–7704.
- 21 L. J. Abbott, C. M. Colina, *J. Chem. Eng. Data.*, 2014, **59**, 3177–3182.
- 22 A. K. Sekizkardes, T. S. Glu, Z. F. Kahveci, H. M. El-Kaderi, *J. Mater. Chem. A*, 2014, **2**, 12492–12500.
- 23 G. Cheng, T. Hasell, A. Trewin, D. J. Adams, A. I. Cooper, *Angew. Chem.*, 2012, **124**, 12899–12903. [10.1039/C9NJ05509F](https://doi.org/10.1039/C9NJ05509F)
- 24 M. G. Rabbani, A. K. Sekizkardes, O. M. El-Kadri, B. R. Kaafarani, H. M. El-Kaderi, *J. Mater. Chem.*, 2012, **22**, 25409–25417.
- 25 M. G. Rabbani, A. K. Sekizkardes, Z. Kahveci, T. E. Reich, R. Ding, H. M. El-Kaderi, *Chem. Eur. J.*, 2013, **19**, 3324–3328.
- 26 V. C. University, T. T. Zhang, H. T. Wang, H. P. Ma, F. X. Sun, X. Q. Cui, G. S. Zhu, *Acta Chim. Sinica*, 2013, **71**, 1598–1602.
- 27 K. V. Rao, R. Haldar, T. K. Maji, S. J. George, *Phys. Chem. Chem. Phys.*, 2016, **18**, 156–163.
- 28 S. Dalapati, S. Jin, J. Gao, Y. Xu, A. Nagai, D. Jiang, *J. Am. Chem. Soc.*, 2013, **135**, 17310–17313.
- 29 G. Cheng, B. Bonillo, R. S. Sprick, D. J. Adams, T. Hasell, A. I. Cooper, *Adv. Funct. Mater.*, 2014, **24**, 5219–5224.
- 30 J. X. Jiang, F. Su, A. Trewin, C. D. Wood, H. Niu, J. T. A. Jones, Y. Z. Khimiyak, A. I. Cooper, *J. Am. Chem. Soc.*, 2008, **130**, 7710–7720.
- 31 X. Y. Wang, C. Zhang, Y. Zhao, S. J. Ren, J. X. Jiang, *Macromol. Rapid Commun.*, 2016, **37**, 323–329.
- 32 C. Y. K. Chan, J. W. Y. Lam, C. K. W. Jim, H. H. Y. Sung, I. D. Williams, B. Z. Tang, *Macromolecules*, 2013, **46**, 9494–9506.
- 33 X. Zhu, C. C. Tian, S. M. Mahurin, S. H. Chai, C. M. L. Wang, S. Brown, Veith, G. M. Luo, M. H, H. L. Liu, S. Dai, *J. Am. Chem. Soc.*, 2012, **134**, 10478–10484.
- 34 R. Gomes, P. Bhanja, A. Bhaumik, *Chem. Commun.*, 2015, **51**, 10050–10053.
- 35 S. H. Xiong, X. Fu, L. Xiang, G. P. Yu, J. G. Guan, Z. G. Wang, Y. Du, X. Xiong, C. Y. Pan, *Polym. Chem.*, 2014, **5**, 3424–3431.
- 36 J. L. Novotney, W. R. Dichtel, *ACS Macro. Lett.*, 2013, **2**, 423–478.
- 37 J. Brandt, J. Schmidt, A. Thomas, J. D. Epping, J. W. Tunable, *Polym. Chem.*, 2011, **2**, 1950–1952.
- 38 S. Ren, M. J. Bojdys, R. Dawson, A. Laybourn, Y. Z. Khimiyak, D. J. Adams, A. I. Cooper, *Porous, Adv. Mater.*, 2012, **24**, 2357–2361.
- 39 J. Jeromenok, J. Weber, *Langmuir*, 2013, **29**, 12982–12989.
- 40 H. Ma, J. J. Chen, L. X. Tan, J. H. Bu, Y. H. Zhu, B. E. Tan, C. Zhang, *ACS Macro. Lett.*, 2016, **5**, 1039–1043.
- 41 Q. Q. Dang, X. M. Wang, Y. F. Zhan and X. M. Zhang, *Polym. Chem.*, 2016, **7**, 643–647.
- 42 Y. F. Chen, H. Sun, R. X. Yang, T. T. Wang, C. J. Pei, Z. T. Xiang, Z. Q. Zhu, W. D. Liang, A. Li, W. Q. Deng, *J. Mater. Chem. A*, 2015, **3**, 87–91.
- 43 S. A, Y. W. Zhang, Z. P. Li, H. Xia, M. Xue, X. M. Liu, Y. Mu, *Chem. Commun.*, 2014, **50**, 8495–8498.
- 44 Z. J. Yan, Y. Yuan, Y. Y. Tian, D. M. Zhang, G. S. Zhu, *Angew. Chem. Int. Ed.*, 2015, **54**, 12733–12737.
- 45 C. Y. Pei, T. Ben, S. X. Xu, S. L. Qiu, *J. Mater. Chem. A*, 2014, **2**, 7179–7187.
- 46 S. Gu, J. Guo, Q. Huang, J. Q. He, Y. Fu, G. C. Kuang, C. Y. Pan, G. P. Yu, *Macromolecules*, 2017, **21**, 8512–8520.
- 47 T. M. Geng, S. N. Ye, Z. M. Zhu, W. Y. Zhang, *J. Mater. Chem. A*, 2018, **6**, 2808–2816.

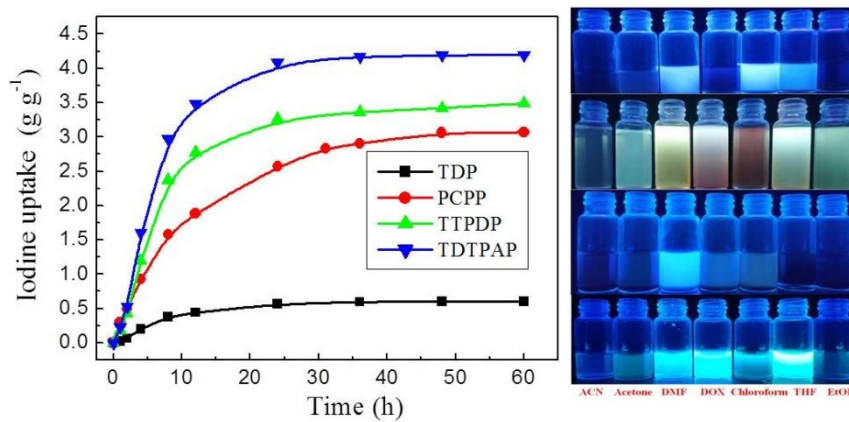
Journal Name

COMMUNICATION

- 48 T. Skorjanc, D. Shetty, S. K. Sharma, J. Raya, H. Traboulsi, D. S. Han, J. Lalla, R. Newlon, R. Jagannathan, S. Kirmizialtin, J.C. Olsen, *Chem. Eur. J.*, 2018, **24**, 1–9.
- 49 M. Janeta, W. Bury, S. Szafert, *ACS Appl. Mater. Interfaces*, 2018, **10**, 19964–19973.
- 50 X.H. Guo, Y. Tian, M.C. Zhang, Y. Li, R. Wen, X. Li, X.F. Li, Y. Xue, L.J. Ma, C.Q. Xia, S.J. Li, *Chem. Mater.*, 2018, **7**, 2299–2308.
- 51 X. Qian, Z. Q. Zhu, H. X. Sun, F. Ren, P. Mu, W. D. Liang, L. H. Chen, A. Li, *ACS Appl. Mater. Interfaces*, 2016, **8**, 21063–21069.
- 52 Y. Z. Liao, J. Weber, B. M. Mills, Z. H. Ren, C. F. J. Fau, *Macromolecules*, 2016, **49**, 6322–6333.
- 53 G. Das, T. Prakasam, S. Nuryyeva, D. S. Han, A. Abdel-Wahab, J. C. Olsen, K. Polychronopoulou, C. Platas-Iglesias, F. Ravoux, M. Jouiad, I. Trabolsi, *J. Mater. Chem. A*, 2016, **4**, 15361–15369.
- 54 L. Guo, X. F. Zeng, D. P. Cao, *Sens. Actuat. B-Chem.*, 2016, **226**, 273–278.
- 55 F. Ren, Z. Q. Zhu, X. Qian, W. D. Liang, P. Mu, H. X. Sun, J. H. Liu, A. Li, *Chem. Commun.*, 2016, **52**, 9797–9800.
- 56 X. F. Wu, H. B. Li, Y. X. Xu, H. Tong, L. X. Wang, *Polym. Chem.*, 2015, **6**, 2305–2311.
- 57 D. X. Ma, B. Y. Li, Z. H. Cui, K. Liu, C. L. Chen, G. H. Li, J. Hua, B. H. Ma, Z. Shi, S. H. Feng, *ACS Appl. Mater. Inter.*, 2016, **8**, 24097–24103.
- 58 Y. K. Li, S. M. Bi, F. Liu, S. Y. Wu, J. Hu, L. M. Wang, H. L. Liu, Y. Hu, *J. Mater. Chem. C*, 2015, **3**, 6876–6881.
- 59 H. P. Ma, B. Li, L. M. Zhang, D. Han, G. S. Zhu, *J. Mater. Chem. A*, 2015, **3**, 19346–19352.
- 60 C. Gu, N. Huang, J. Gao, F. Xu, Y. H. Xu, D. L. Jiang, *Angew. Chem.*, 2014, **126**, 4950–4955.
- 61 T. M. Geng, W. Y. Zhang, Z. M. Zhu, X. M. Kai, *Micropor. Mesopor. Mat.*, 2019, **273**, 163–170.
- 62 Z. Chen, M. Chen, Y. L. Yu, L. M. Wu, *Chem. Commun.*, 2017, **53**, 1989–1992.

View Article Online
DOI: 10.1039/C9NJ05509F

Graphical Abstract

View Article Online
DOI: 10.1039/C9NJ05509F1
2
3
4
5
6
7
8
9
10
11
12
13
14
15
16
17
18
19
20
21
22
23
24
25
26
27
28
29
30
31
32
33
34
35
36
37
38
39
40
41
42
43
44
45
46
47
48
49
50
51
52
53
54
55
56
57
58
59
60